Interference Effects in the Resonant Photoemission Channels to the Ne^+ $2p^4(^1D_2)3p\ ^2P$, ^2D, and ^2F States in the Ne 1s Excitation Region

A. De Fanis,[1] N. Saito,[2] H. Yoshida,[3] Y. Senba,[3] Y. Tamenori,[4] H. Ohashi,[4] H. Tanaka,[5] and K. Ueda[1,*]

[1]*Institute of Multidisciplinary Research for Advanced Materials, Tohoku University, Sendai 980-8577, Japan*
[2]*National Institute of Advanced Industrial Science and Technology, Tsukuba 305-8568, Japan*
[3]*Department of Physical Science, Hiroshima University, Higashi-Hiroshima 739-8526, Japan*
[4]*Japan Synchrotron Radiation Institute, Sayo-gun, Hyogo 679-5198, Japan*
[5]*Department of Physics, Sophia University, Tokyo 102-8554, Japan*

(Received 26 March 2002; published 25 November 2002)

We present measurements of total and partial photoionization cross sections of Ne in the 1s excitation region. The total cross section exhibits resonances with symmetric profiles, whereas the branching ratios to the Ne^+ $2p^4(^1D_2)3p\ ^2P$, ^2D, and ^2F states present strong oscillations in the interresonance regions. We prove that not only the interference between the direct and resonant ionization processes but also the interference among the ionization processes via different nonisolated resonances are important for this effect.

DOI: 10.1103/PhysRevLett.89.243001 PACS numbers: 32.30.Rj, 32.80.Hd, 32.80.Fb

The wave nature of electrons, described by Schrödinger's equation, manifests itself via various interference effects in photoelectric phenomena. One of the typical examples is the interference between direct and resonant photoemission pathways. In analogy to Young's two-slit experiment, the photoelectron waves passing through these two different pathways interfere with each other and result in the asymmetric profile of the resonance in the photoabsorption cross section [1], as observed frequently in valence-shell photoabsorption in the vacuum-ultraviolet region (see, for example, [2]). Such interference effects were generally neglected in the analysis of x-ray absorption processes where the inner-shell excitation takes places [3]. Recent inner-shell photoemission measurements, however, revealed that, although the photoabsorption spectra show symmetric resonant profiles, the partial cross sections for ionization to specific ionic states can present asymmetric resonant profiles intrinsic of the final states [4–7]. Analysis of the asymmetric profiles in the partial cross sections has generally been limited to the decay of one isolated resonance [4–9].

In the present work, we have investigated total and partial cross sections for photoionization of Ne in the 1s excitation region using high photon and electron energy resolution. We present evidence that interference between resonant ionization processes through different nonisolated resonances plays an important role.

The experiment has been performed at the c-branch of beam line 27SU [10,11] at SPring-8 in Japan. The total cross section σ is measured by collecting the total ion yield. For such measurements the photon energy width (full width at half maximum, FWHM) is set to $\Delta h\nu \sim 66$ meV, as estimated from Xe 5p photoemission spectra. The total cross section thus measured is presented in Fig. 1, together with a least-χ^2 fit (see below). The photon energy scale in Fig. 1 is calibrated by using the energies of the $1s^{-1}3p$ and $1s^{-1}4p$ resonances reported in Ref. [12]. This spectrum is similar to the one presented in Ref. [12], but the present resolution is slightly higher, and thus the $1s^{-1}6p$ resonance is resolved.

X-ray absorption cross sections in the inner-shell excitation regions are normally analyzed with the following expression [3]:

$$\sigma = \sigma_{\mathrm{dir}} + \sum_n \frac{\sigma_n}{1+\epsilon_n^2} + \sigma_{1s}, \qquad (1)$$

where n labels the resonances and $\epsilon_n = 2(h\nu - E_n)/\Gamma_n$ are the distances of the photon energy $h\nu$ from the resonant energies E_n measured in terms of half natural widths $\Gamma_n/2$. σ_n and σ_{dir} are the cross sections for the resonant and nonresonant ionization. $\Gamma_n/2$, σ_n, and σ_{dir} are considered constant in the energy interval of interest. The term σ_{1s} in (1) represents the 1s ionization cross

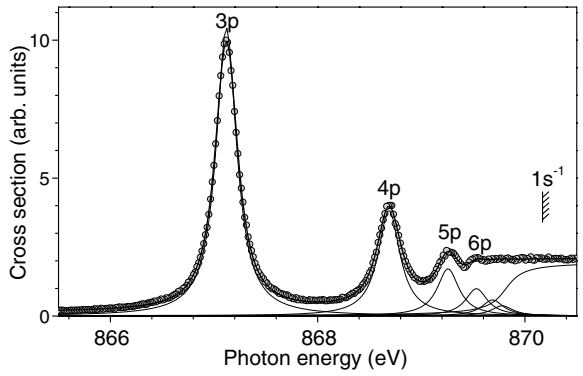

FIG. 1. Circles: measured total cross section for photoionization of Ne in the energy region of the 1s excitations. Thick line: least-χ^2 fit based on Lorentzian profiles, convoluted with a Gaussian profile with FWHM fixed to 66 meV. Thin lines: contributions from the individual resonances, before the convolution.

section:

$$\sigma_{1s} \propto \frac{1}{2} + \frac{1}{\pi}\arctan[2(h\nu - E_{1s})/\Gamma]. \quad (2)$$

Each Lorentzian component in Eq. (1) is the limit $q \to +\infty$, but $\sigma_a q^2$ is still finite for the profile of Fano [1]:

$$\sigma = \sigma_b + \sigma_a \frac{(q+\epsilon)^2}{1+\epsilon^2}. \quad (3)$$

Here q is the Fano's profile index, σ_a and σ_b are the cross sections for excitation of the continuum that does and does not interact with the discrete isolated resonance. Although the interaction of the resonances with the continuum may not be negligible (see below), the Lorentzian profiles are still a good approximation for the resonant profiles in the total cross section.

In the fitting routine, the expression (1) is convoluted with a Gaussian profile with fixed FWHM of 66 meV in order to simulate the photon bandpass. The fit extracts the line strengths, Lorentzian widths, and energies of the resonances. Although $1s^{-1}7p$ and $1s^{-1}8p$ cannot be resolved, they are also included in the fit, in order to reach an overall better agreement between the fit and the measurement. Contributions from higher members are included in σ_{1s}. Some parameters are fixed using quantum defect methods [13]. Namely, the energies of the $1s^{-1}6p - 1s^{-1}8p$ resonances are fixed to the values extrapolated from the $1s^{-1}3p$–$1s^{-1}5p$ resonances, whereas the line strengths of $1s^{-1}7p$ and $1s^{-1}8p$ relative to the line strength of $1s^{-1}6p$ are fixed. The widths are assumed to be the same for the resonances $1s^{-1}4p$–$1s^{-1}8p$. The widths for these high-n members, however, turn out to be the same as that of $1s^{-1}3p$ via fitting within the experimental uncertainties. The value thus obtained for the natural lifetime width, $\Gamma_{3p} = 240 \pm 10$ meV, is slightly lower than the calculated one in Ref. [12], $\Gamma_{3p} = 258$ meV.

We now describe the measurements of partial cross sections. Electron emission to the $2p^4(^1D_2)3p$, ^2P, ^2D, and ^2F states are observed at various photon energies in the Ne $1s$ excitation region. The electron spectrometer employed is a high-resolution hemispherical analyzer (Gammadata Scienta SES-2002) coupled via an electrostatic lens to a gas cell. In the electron spectra the photon band width and the electron kinetic energy width are set to ~66 and ~33 meV, respectively, whereas the Doppler broadening due to thermal motion of the sample gas atoms in the cell at room temperature is ~80 meV. Electron spectra are collected for both 0° and 90° of emission relative to the polarization vector of the incident light. The angle-integrated spectra are obtained from the 0° and 90° spectra after correction for photon flux intensity and degree of linear polarization (see [14] for a general expression). At photon energies where the electron count rates are low, the acquisition time is increased, so that measurements at all photon energies have enough statistics to extract the line strengths with sufficiently small uncertainties.

Figure 2 shows two examples of angle-integrated electron spectra recorded at two photon energies close to the one for the minimum of the cross section between the $3p$ and $4p$ resonances. The error bars contain only the statistical contributions as propagated from the number of counts in the original spectra. From the spectra in Fig. 2, the line strength of each component is extracted by a least-χ^2 fit with Gaussian profiles. Gaussian profiles are chosen because in the electron spectra the broadening caused by instrumental and Doppler effects is much larger than the natural lifetime width of the valence-ionized final states. In the fit, the separations between the states are fixed at the values obtained from the spectra recorded at the peak of the $1s^{-1}3p$ resonance, which are identical to the values in Ref. [15]. The values of the branching ratios for the ^2P, ^2D, and ^2F components extracted from the spectra in Figs. 2(a) and 2(b) are $0.15 \pm 0.02{:}0.35 \pm 0.02{:}0.50 \pm 0.02$ and $0.44 \pm 0.03{:}0.27 \pm 0.03{:}0.29 \pm 0.02$, respectively. The photon energy changes only 190 meV, but these branching ratios are quite different from each other, indicating that they are very sensitive to the excitation energy.

The measured partial cross sections, i.e., the spectral behavior of the line strengths for the ^2P, ^2D, and ^2F components extracted from the fitting to the electron spectra as in Fig. 2, are displayed in Fig. 3(a). Like in the total cross section, the $1s^{-1}3p$ resonance shows nearly symmetric profiles in each partial cross section. This may be a first indication that the interference effects are weak, and at this point one may be tempted to conclude that no evidence of large interference effects can be extracted from the present data. Now we focus on the key result of this work. The branching ratios for the three components are plotted in Fig. 3(b) as a function of excitation energy. The branching ratios for ^2P and ^2F exhibit oscillations, with pronounced minima and maxima in the energy regions between the resonances. The amplitudes of the

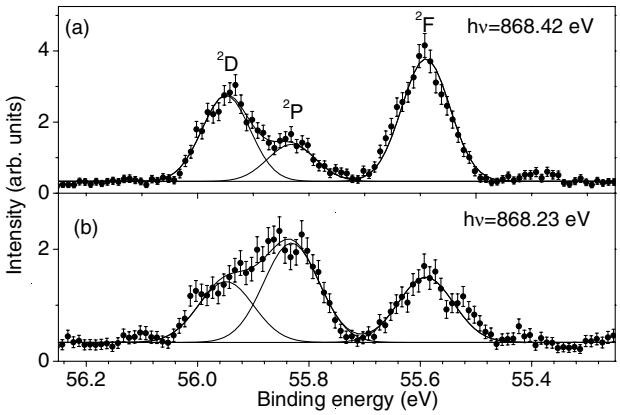

FIG. 2. Angle-integrated electron spectra measured at the photon energies of (a) 868.42 and (b) 868.23 eV, together with the fit by Gaussian profiles.

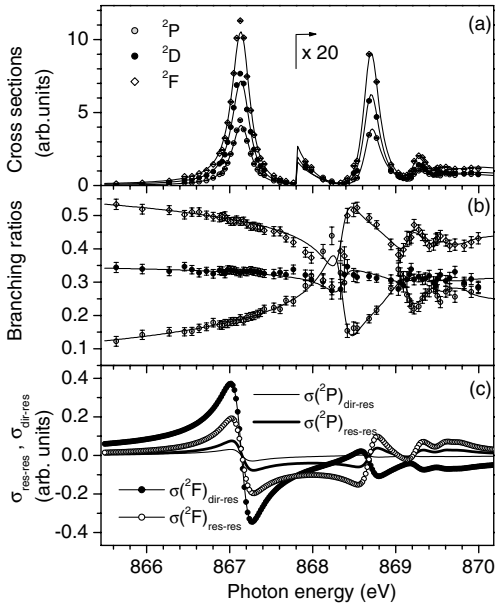

FIG. 3. (a) Measurements of the partial cross sections to $2p^4(^1D_2)3p\ ^2P$, ^2D, and ^2F together with the fit of individual components. (b) Branching ratios extracted from the measured electron spectra (points), and from the corresponding fit (lines). (c) Contributions of $\sigma_{\text{res-res}}$ and $\sigma_{\text{dir-res}}$ as extracted from the analysis of the partial cross sections for the ^2P and ^2F states.

oscillations are certainly larger than the uncertainties of the data points. The oscillations stem from the fact that each of the three partial cross sections reaches a minimum, at energies different from one another, in the interresonance regions.

To analyze the partial cross sections which exhibit the interference effects, we start with the model of Ref. [8]. The amplitude for each specific continuum channel α in the region of one isolated resonance is written as follows:

$$A_\alpha = d_\alpha + \mathcal{D}_\alpha \frac{q + \epsilon}{i + \epsilon}, \tag{4}$$

where d_α and $\mathcal{D}_\alpha$ are the dipole amplitudes of the direct and resonant processes. This model is equivalent to the one developed by Starace [9]. The square modulo of Eq. (4) can be written in the form of Fano:

$$|A_\alpha|^2 = \sigma_{a\alpha} + \sigma_{b\alpha} \frac{(q_\alpha + \epsilon)^2}{1 + \epsilon^2}, \tag{5}$$

provided $\sigma_{a\alpha}$, $\sigma_{b\alpha}$, and q_α are appropriately defined. Note that q in Eq. (4) is the same as in Eq. (3), whereas q_α in Eq. (5) is different. We generalize Eq. (4) to the case of more than one resonance in the following way:

$$A_\alpha = d_\alpha + \sum_n \mathcal{D}_{n\alpha} \frac{q_n + \epsilon_n}{i + \epsilon_n}. \tag{6}$$

Unlike in the original model of Fano, the resonances in Eq. (6) are not considered isolated.

Following the result that the resonance profiles in the total cross section σ are symmetric, we replace Eq. (6) with its limit $q_n \to +\infty$ but $D_{n\alpha} = q_\alpha \mathcal{D}_{n\alpha}$ still finite:

$$A_\alpha = d_\alpha + \sum_n \frac{D_{n\alpha}}{i + \epsilon_n}. \tag{7}$$

This is the same expression as the one that Saito *et al.* [16] employed for the analysis of relative partial cross sections to Ne^+ $2p^4(^1D_2)3p$ and $2p^4(^1D_2)4p$ in the region of the $1s^{-1}3p$ resonance.

In this model each channel α is defined by the final ionic state i and by the angular momentum l of the outgoing electron, $\alpha \equiv (i, l)$, as in Ref. [8]. We assume the *LSJ*-coupling scheme, which is considered to be valid in the description of the Ne $1s$ excitation and decay [15]. Then each partial cross section σ_i corresponds to the incoherent sum of the two different photoelectron channels $l = 0, 2$. Thus each partial cross section is parametrized as follows:

$$\sigma_i = A_i + B_i \sum_n \frac{R_n^2}{1 + \epsilon_n^2} + \sigma_{\text{dir-res}} + \sigma_{\text{res-res}} + \sigma_{1s,i} \tag{8}$$

with R_n normalized so that R_{3p} is unity. The direct-resonant $\sigma_{\text{dir-res}}$ and resonant-resonant $\sigma_{\text{res-res}}$ interference terms are as follows:

$$\sigma_{\text{dir-res}} = 2C_i \sum_m \frac{R_m \epsilon_m}{1 + \epsilon_m^2} \tag{9}$$

and

$$\sigma_{\text{res-res}} = 2B_i \sum_{m<n} \frac{R_m R_n (1 + \epsilon_m \epsilon_n)}{(1 + \epsilon_m^2)(1 + \epsilon_n^2)}. \tag{10}$$

A_i, B_i, and C_i are defined as

$$A_i = \sum_{l=0,2} d_{i,l}^2, \tag{11}$$

$$B_i R_m R_n = \sum_{l=0,2} D_{m,i,l} D_{n,i,l}, \tag{12}$$

$$C_i R_n = \sum_{l=0,2} d_{i,l} D_{n,i,l}. \tag{13}$$

$\sigma_{1s,i}$ described by the same analytic form as Eq. (2) expresses the contributions from high $1s^{-1}np$ ($n \geq 9$) members as well as from the $1s$ ionization.

The electron spectra recorded at the peak of each resonance show almost the same branching ratios, close to the statistical ratios expected within the *LSJ*-coupling scheme: B_{2P}:B_{2D}:B_{2F} = 3:5:7. We thus assume that different resonances have the same branching ratios over different final states. This makes B_i well defined in Eq. (12). In general, from Eqs. (11)–(13), A_i, B_i, C_i are constrained to fulfill the inequality $A_i B_i \geq C_i^2$. However, by using the spectator model within the *LSJ*-coupling scheme, the photoelectron wave is restricted to $l = 2$. Then we have $A_i B_i = C_i^2$.

The partial cross sections in Fig. 3(a) are fitted simultaneously using the model described above. In the fitting, the spectra described by Eq. (8) are broadened by convolution with a Gaussian profile with width fixed to 66 meV to simulate the photon bandpass. As can be seen in Fig. 3(a), the fit reproduces well the measurements. The continuous lines superimposed to the measured branching ratios in Fig. 3(b) are not the results of an additional fit but the branching ratios calculated from the three simultaneous fits for the partial cross sections in Fig. 3(a). The agreement between the continuous lines and the experimental points is reasonable.

Consider the origin of the interference effects. In the expression (8), the two terms $\sigma_{\text{dir-res}}$ and $\sigma_{\text{res-res}}$ contribute to the interference. Note the different origin of $\sigma_{\text{dir-res}}$ and $\sigma_{\text{res-res}}$: the former corresponds to the interference between direct and resonant processes, whereas the latter is due to the interference between resonant photoionization through different resonances. The $\sigma_{\text{res-res}}$ term is negligible if the resonances are isolated, i.e., if $|E_n - E_m| \gg \Gamma$. Then a linear combination of Eq. (5) is appropriate to analyze the partial cross sections. If the resonances are not isolated, i.e., if $|E_n - E_m| \sim \Gamma$, the $\sigma_{\text{res-res}}$ term is important in the interresonance regions and the effect due to this term becomes observable. In Fig. 3(c) we present $\sigma_{\text{res-res}}$ and $\sigma_{\text{dir-res}}$ for the ^2P and ^2F states, calculated from the parameters obtained by the fitting described above. The $\sigma_{\text{res-res}}$ contribution to the partial cross section is as strong as or even stronger than $\sigma_{\text{dir-res}}$ in the interresonance regions. Because of this negative interference term, each partial cross section goes close to zero in the region between the $1s^{-1}3p$ and $1s^{-1}4p$ resonances where the branching ratios change significantly.

Consider how these two interference terms play their roles in describing the oscillations in the branching ratios. If the direct process is absent for all the channels, i.e., if $A_i = C_i = 0$ for $i = {}^2P, {}^2D, {}^2F$, as Rubensson *et al.* assumed in the analysis of the branching ratios to the Ne^+ $2p^{-2}np$ states with different n [17], the branching ratios to the Ne^+ $2p^{-2}(^1D_2)3p$, ^2P, ^2D, and ^2F states become constant in the present model, because the branching ratios are then solely determined by B_i. If the direct process is present, then the energy for the minimum of the cross section varies depending on the ratio between A_i and B_i. Thus it is clear that the direct-resonant interference term is essential in describing the oscillations of the branching ratios. On the other hand, if the resonant-resonant interference term is switched off, each partial cross section does not go close to zero any more in the interresonance regions, and thus the amplitudes of the oscillations are significantly suppressed. Indeed, attempts to fit the partial cross sections with the Fanolike profiles (5) fail to reproduce the large oscillations of the branching ratios in the interresonance regions. This is a clear indication that the $\sigma_{\text{res}-\text{res}}$ terms are important; i.e., the resonances are not isolated.

In conclusion, we presented the absorption cross section of Ne in the region of $1s$ excitations with the highest resolution ever recorded. This allowed us to resolve the $1s^{-1}6p$ resonance and to extract the improved value of the natural lifetime width $\Gamma \sim 240 \pm 10$ meV for the $1s^{-1}3p$ state. Although measurements of total and partial cross sections seem to indicate that interference effects are weak in photoemission to the $2p^4(^1D_2)3p\,^2P$, ^2D, and ^2F states, the relative branching ratios present large oscillations. We proved that not only the interference between the direct and resonant ionization processes, but also the interference among the resonant ionization processes via nonisolated resonances play important roles for the appearance of oscillations in the branching ratios. Because of its generality, we expect the interference among multiple pathways reported here, i.e., the direct photoemission pathway and more than one resonant photoemission pathways via nonisolated resonances, to be present not only in other atomic resonant photoemission but also in molecular resonant photoemission, as well as in resonant photoemission from condensed matter, in the inner-shell excitation regions.

This experiment was carried out with the approval of the SPring-8 program advisory committee and supported in part by Grants-in-Aid for Scientific Research from the Japan Society for the Promotion of Science (JSPS). We thank N. M. Kabachnik, U. Hergenhahn, and U. Becker for useful discussions. A. D. is grateful to JSPS for financial support.

*Corresponding author.
Email address: ueda@tagen.tohoku.ac.jp

[1] U. Fano, Phys. Rev. **124**, 1866 (1961); U. Fano and J.W. Cooper, Phys. Rev. **137**, A1364 (1965).
[2] R. P. Madden and K. Codling, Phys. Rev. Lett. **10**, 516 (1963).
[3] M. Breinig *et al.*, Phys. Rev. A **22**, 520 (1980).
[4] R. Camilloni *et al.*, Phys. Rev. Lett. **77**, 2646 (1996).
[5] S. E. Canton-Rogan *et al.*, Phys. Rev. Lett. **85**, 3113 (2000).
[6] R. R. T. Marinho *et al.*, Phys. Rev. A **63**, 032514 (2001).
[7] O. Nayandin *et al.*, Phys. Rev. A **64**, 022505 (2001).
[8] N. M. Kabachnik and I. P. Sazhina, J. Phys. B **9**, 1681 (1976).
[9] A. F. Starace, Phys. Rev. A **16**, 231 (1977).
[10] H. Ohashi *et al.*, Nucl. Instrum. Methods Phys. Res., Sect. A **467**, 529 (2001).
[11] H. Ohashi *et al.*, Nucl. Instrum. Methods Phys. Res., Sect. A **467**, 533 (2001).
[12] M. Coreno *et al.*, Phys. Rev. A **59**, 2494 (1999).
[13] U. Fano and J.W. Cooper, Rev. Mod. Phys. **40**, 441 (1968).
[14] A. De Fanis *et al.*, Surf. Rev. Lett. **9**, 51 (2002).
[15] Y. Shimizu *et al.*, J. Phys. B **33**, L685 (2000).
[16] N. Saito *et al.*, J. Phys. B **33**, L729 (2000).
[17] J.-E. Rubensson *et al.*, Chem. Phys. Lett. **257**, 447 (1996).